Coupling of nitrogen-vacancy centers in a nanodiamond to a silver nanocube

Andersen, Sebastian Kim Hjælm; Kumar, Shailesh; Bozhevolnyi, Sergey I.

Published in:
Optical Materials Express

DOI:
10.1364/OME.6.003394

Publication date:
2016

Document version
Publisher's PDF, also known as Version of record

Citation for pulished version (APA):
Andersen, S. K. H., Kumar, S., & Bozhevolnyi, S. I. (2016). Coupling of nitrogen-vacancy centers in a nanodiamond to a silver nanocube. Optical Materials Express, 6(11), 3394-3406. DOI: 10.1364/OME.6.003394

Research Article | Vol. 6, No. 11 | 1 Nov 2016 | OPTICAL MATERIALS EXPRESS 3394

Optical Materials EXPRESS

Coupling of nitrogen-vacancy centers in a nanodiamond to a silver nanocube

SEBASTAIN K. H. ANDERSEN,* SHAILESH KUMAR, AND SERGEY I. BOZHEVOLNYI

Centre for Nano Optics, University of Southern Denmark, Campusvej 55, DK-5230 Odense M, Denmark
**sekh@iti.sdu.dk*

Abstract: Spontaneous emission (SE) of nitrogen-vacancy centers (NV-centers), which are contained in a single nanodiamond (ND), placed near a silver nanocube, is investigated both experimentally and theoretically. The ND-cube system is assembled with an atomic force microscope, allowing us to directly compare its SE properties to that of the isolated ND. It is demonstrated that the cube coupled NV-centers exhibit strongly polarized SE. For optimal pump laser polarization, the rate of photons is enhanced by a factor of 4.1, with the excited state lifetime being reduced by a factor of 4.1. The enhancement of photon rate is a consequence of local field enhancement of the pump laser, while the SE polarization and lifetime reduction results from coupling of NV-centers to the localized surface plasmon mode of the nanocube. The experimental observations are in qualitative agreement with the model of SE from randomly oriented electric dipoles, allowing us to reveal the underlying physics of the investigated configuration.

OCIS codes: (270.0270) Quantum optics; (260.3910) Metal optics; (160.2540) Fluorescent and luminescent materials; (230.6080) Sources.

References and links

1. B. Lounis and M. Orrit, "Single-photon sources," Rep. Prog. Phys. **68**, 1129 (2005).
2. I. A. Walmsley, "Quantum optics: Science and technology in a new light," Science **348**, 525–530 (2015).
3. J. G. Rarity, P. C. M. Owens, and P. R. Tapster, "Quantum Random-number Generation and Key Sharing," J. Mod. Opt. **41**, 2435–2444 (1994).
4. A. Beveratos, R. Brouri, T. Gacoin, A. Villing, J. Poizat, and P. Grangier, "Single Photon Quantum Cryptography," Phys. Rev. Lett. **89**, 187901 (2002).
5. M. Pelton, "Modified spontaneous emission in nanophotonic structures," Nat. Photon. **9**, 427–435 (2015).
6. E. M. Purcell, "Spontaneous emission probabilities at radio frequencies," Phys. Rev. **69**, 681 (1946).
7. A. Kinkhabwala, Z. Yu, Y. Avlasevich, K. Mullen, and W. E. Moerner, "Large single-molecule fluorescence enhancements produced by a bowtie nanoantenna," Nat. Photon. **3**, 654–657 (2009).
8. V. I. Kukushkin, I. M. Mukhametzhanov, I. V. Kukushkin, V. D. Kulakovskii, I. V. Sedova, S. V. Sorokin, A. A. Toropov, S. V. Ivanov, and A. S. Sobolev, "Control of semiconductor quantum dot emission intensity and polarization by metal nanoantennas," Phys. Rev. B **90**, 235313 (2014).
9. A. Huck, S. Kumar, A. Shakoor, and U. L. Andersen, "Controlled Coupling of a Single Nitrogen-Vacancy Center to a Silver Nanowire," Phys. Rev. Lett. **106**, 096801 (2011).
10. E. Bermudez-Urena, C. Gonzalez-Ballestero, M. Geiselmann, R. Marty, I. P. Radko, T. Holmgaard, Y. Alaverdyan, E. Moreno, F. J. Garcia-Vidal, S. I. Bozhevolnyi, and R. Quidant, "Coupling of individual quantum emitters to channel plasmons," Nat. Commun. **6**, 7883 (2015).
11. A. G. Curto, G. Volpe, T. H. Taminiau, M. P. Kreuzer, R. Quidant, and N. F. van Hulst, "Unidirectional Emission of a Quantum Dot Coupled to a Nanoantenna," Science **329**, 930–933 (2010).
12. G. M. Akselrod, C. Argyropoulos, T. B. Hoang, C. CiracÃň, C. Fang, J. Huang, D. R. Smith, and M. H. Mikkelsen, "Probing the mechanisms of large Purcell enhancement in plasmonic nanoantennas," Nat. Photon. **8**, 835–840 (2014).
13. S. J. P. Kress, F. V. Antolinez, P. Richner, S. V. Jayanti, D. K. Kim, F. Prins, A. Riedinger, M. P. C. Fischer, S. Meyer, K. M. McPeak, D. Poulikakosand, and D. J. Norris, "Wedge Waveguides and Resonators for Quantum Plasmonics," Nano Lett. **15**, 6267–6275 (2015).
14. J. Gerard and B. Gayral, "Strong Purcell effect for InAs quantum boxes in three-dimensional solid-state microcavities," J. Lightwave Technol **17**, 2089–2095 (1999).
15. F. Wang and Y. R. Shen, "General Properties of Local Plasmons in Metal Nanostructures," Phys. Rev. Lett. **97**, 206806 (2006).
16. K. Chen, V. P. Drachev, J. D. Borneman, A. V. Kildishev, and V. M. Shalaev, "Drude Relaxation Rate in Grained Gold Nanoantennas," Nano Lett. **10**, 916–922 (2010).

#275630 http://dx.doi.org/10.1364/OME.6.003394
Journal © 2016 Received 12 Sep 2016; revised 29 Sep 2016; accepted 29 Sep 2016; published 5 Oct 2016

Optical Materials EXPRESS

17. V. P. Drachev, U. K. Chettiar, A. V. Kildishev, H. Yuan, W. Cai, and V. M. Shalaev, "The Ag dielectric function in plasmonic metamaterials," Opt. Express **16**, 1186–1195 (2008).
18. M. Bosman, L. Zhang, H. Duan, S. F. Tan, C. A. Nijhuis, C. Qiu, and J. K. W. Yang, "Encapsulated Annealing: Enhancing the Plasmon Quality Factor in Lithographically Defined Nanostructures," Sci. Rep. **4**, 5537 (2014).
19. N. P. de Leon and B. J. Shields and C. L. Yu, D. E. Englund, A. V. Akimov, M. D. Lukin, and H. Park, "Tailoring Light-Matter Interaction with a Nanoscale Plasmon Resonator," Phys. Rev. Lett. **108**, 226803 (2012).
20. T. B. Hoang, G. M. Akselrod, and M. H. Mikkelsen, "Ultrafast Room-Temperature Single Photon Emission from Quantum Dots Coupled to Plasmonic Nanocavities," Nano Lett. **16**, 270–275 (2015).
21. S. K. H. Andersen, A. Pors, and S. I. Bozhevolnyi, "Gold Photoluminescence Wavelength and Polarization Engineering," ACS Photonics **2**, 432–438 (2015).
22. Y. Alaverdyan, N. Vamivakas, J. Barnes, C. Lebouteiller, J. Hare, and M. Atatüre, "Spectral tunability of a plasmonic antenna with a dielectric nanocrystal," Opt. Express **19**, 18175–18181 (2011).
23. P. Anger, P. Bharadwaj, and L. Novotny,"Enhancement and Quenching of Single-Molecule Fluorescence," Phys. Rev. Lett. **96**, 113002 (2006).
24. K. H. Drexhage,"Influence of a dielectric interface on fluorescence decay time," JOL **1-2**, 693–701 (1970).
25. G. W. Ford and W. H. Weber,"Electromagnetic interactions of molecules with metal surfaces," Phys. Rep. **113**, 195–287 (1984).
26. A. Pors and S. I. Bozhevolnyi,"Quantum Emitters near Layered Plasmonic Nanostructures: Decay Rate Contributions," ACS Photonics **2**, 228–236 (2015).
27. S. Schietinger, M. Barth, T. Aichele, and O. Benson,"Plasmon-Enhanced Single Photon Emission from a Nanoassembled Metal-Diamond Hybrid Structure at Room Temperature," Nano Lett. **9**, 1694–1698 (2009).
28. M. Geiselmann, R. Marty, J. Renger, F. J. G. de Abajo, and R. Quidant,"Deterministic Optical-Near-Field-Assisted Positioning of Nitrogen-Vacancy Centers," Nano Lett. **14**, 1520–1525 (2014).
29. A. W. Schell, G. Kewes, T. Hanke, A. Leitenstorfer, R. Bratschitsch, O. Benson, and T. Aichele,"Single defect centers in diamond nanocrystals as quantum probes for plasmonic nanostructures," Opt. Express **19**, 7914–7920 (2011).
30. T. T. Tran, J. Fang, H. Zhang, P. Rath, K. Bray, R. G. Sandstrom, O. Shimoni, M. Toth, and I. Aharonovich, "Facile Self-Assembly of Quantum Plasmonic Circuit Components," Adv. Mater. **27**, 4048–4053 (2015).
31. A. Gruber, A. Dräbenstedt, C. Tietz, L. Fleury, J. Wrachtrup, and C. von Borczyskowski, "Scanning Confocal Optical Microscopy and Magnetic Resonance on Single Defect Centers," Science **276**, 2012–2014 (1997).
32. F. A. Inam, M. D. W. Grogan, M. Rollings, T. Gaebel, J. M. Say, C. Bradac, T. A. Birks, W. J. Wadsworth, S. Castelletto, J. R. Rabeau, and M. J. Steel, "Emission and Nonradiative Decay of Nanodiamond NV Centers in a Low Refractive Index Environment," ACS Nano **7**, 3833–3843 (2013).
33. A. Mohtashami and A. F. Koenderink,"Suitability of nanodiamond nitrogenâĂŞvacancy centers for spontaneous emission control experiments," New J. Phys. **15**, 043017 (2013).
34. S. Zhang, K. Bao, N. J. Halas , H. Xu, and P. Nordlander, "Substrate-Induced Fano Resonances of a Plasmonic Nanocube: A Route to Increased-Sensitivity Localized Surface Plasmon Resonance Sensors Revealed," Nano Lett. **11**, 1657–1663 (2011).
35. J. M. Taylor, P. Cappellaro, L. Childress, L. Jiang, D. Budker, P. R. Hemmer, A. Yacoby, R. Walsworth, and M. D. Lukin, "High-sensitivity diamond magnetometer with nanoscale resolution," Nat. Phys. **4**, 810-816 (2008).
36. T. Wolf, P. Neumann, K. Nakamura, H. Sumiya, T. Ohshima, J. Isoya, and J. Wrachtrup, "Subpicotesla Diamond Magnetometry," Phys. Rev. X **5**, 041001 (2015).
37. M. W. Doherty, J. Michl, F. Dolde I. Jakobi, P. Neumann, N. B. Manson, and J Wrachtrup,"Measuring the defect structure orientation of a single NV-centre in diamond," New J. Phys. **16**, 063067 (2014).
38. K. C. Fu, C. Santori, P. E. Barclay, L. J. Rogers, N. B. Manson, and R. G. Beausoleil,"Observation of the Dynamic Jahn-Teller Effect in the Excited States of Nitrogen-Vacancy Centers in Diamond," Phys. Rev. Lett. **103**, 256404 (2009).
39. L. Novotny and B. Hecht, *Principles of Nano-Optics* (Cambridge University, 2006).
40. P. B. Johnson and R. W. Christy,"Optical Constants of the Noble Metals," Phys. Rev. B **6**, 4370–4379 (1972).
41. I. H. Malitson,"Interspecimen Comparison of the Refractive Index of Fused Silica," J. Opt. Soc. Am. **55**, 1205–1209 (1965).
42. C. Ropp, Z. Cummins, S. Nah, J. T. Fourkas, B. Shapiro, and E. Waks, "Nanoscale probing of image-dipole interactions in a metallic nanostructure," Nat. Commun. **6**, 6558 (2015).

1. Introduction

Efficient single photon source [1] is an enabling technology for quantum technological schemes, exploiting the quantum nature of light [2–4]. The realization of such a device requires controlling the spontaneous emission (SE) of a bright photostable quantum emitter [5]. Based on the pioneering work of Purcell [6], efforts towards this goal typically consist of coupling the quantum emitter, such as a molecule, quantum dot or diamond color center to engineered electromagnetic modes e.g. resonator- or waveguide mode [7–10]. The coupling of emitters to a resonator

Optical Materials EXPRESS

mode has previously been demonstrated to allow for modification of the excited state lifetime, spectral distribution and spatial SE pattern [11–13]. The potential coupling rate is optimized by maximizing the quality factor to mode volume ratio of the resonant mode [14]. Generally, the resonator design is optimized by two approaches: a low-loss all dielectric approach with approximately diffraction limited mode volume or resonant metal nanostructures supporting strongly confined plasmonic modes with quality factors limited by the intrinsic losses in metal [15]. In the pursuit of limiting the influence of extrinsic loss factors such as grain boundaries, surface roughness and lattice defects [16–18] of the metal, recent works have demonstrated the potential of implementing atomically smooth chemically synthesized monocrystalline metal nanoparticles in resonator configurations [19, 20]. Silver is typically the metal of choice for such configurations, given the low loss and absence of background metal fluorescence (for 532nm pump), which problematically mimic enhancement effects observed for quantum emitters [21,22]. The probability of a quantum emitter decaying to the resonator mode, free radiation or non-radiative loss, respectively, is strongly dependent on the emitter position and the orientation of its dipole moment [23–26]. The well-controlled coupling of emitters to metal nanoparticles requiring accurate emitter positioning and orientation is therefore a strong focus in current plasmonic research [27–30]. Excellent results have previously been achieved by coupling either molecules or quantum dots to silver nanocubes [12, 20], however, these demonstrations suffer from photobleaching of the emitter, thus limiting long-term use. A promising emitter to remedy this issue is the nitrogen-vacancy center (NV-center) in diamond, given its photostable SE at room temperature [31]. However, quantifying the influence of resonator effects on the SE properties of NV-centers contained inside a single nanodiamond (ND) is challenging, with conventional use of reference samples, due to the large ND-to-ND spread in lifetime and brightness [32, 33].

In this work, we directly quantify the changed SE properties of NV-centers in close proximity to a monocrystalline silver nanocube, relative to a dielectric environment, by deterministic assembly of a single ND-cube system using an atomic force microscope (AFM). The system yields a background-free response for which the localized surface plasmon (LSP) mode of the cube is well confined near the substrate, given the strong substrate-particle interaction for this specific particle geometry [34]. In order to probe the range of NV-center responses, given the strong dependence on position and dipole orientation, we initially consider the case of a ND containing multiple emitters (∼15), coupled to a silver nanocube. The system exhibits strongly polarized SE, with an enhanced photon rate, strongly dependent on the pump polarization, reaching a lifetime reduction of a factor 4.1 (and corresponding photon rate enhancement of 4.1) under optimal pump polarization. The experimental results are in qualitative agreement with modelling, which allows us to identify governing parameters for the overall experimental observations. Finally we demonstrate the consistency of our results for a ND-cube system containing few emitters (1-2). The results provide a foundation for the optimization of SE properties of more complex cube-based photon sources and may find applications within nanometer scale magnetometry based on single or NV-center ensembles, for which optical read-out of the ground spin state is essential [35, 36].

2. Experiment, results and discussion

The sample was prepared by introducing gold reference marks on a low fluorescence fused silica substrate (SPI supplies) by standard electron beam lithography. The marks allowed for easy identification of a specific ND, in both AFM and fluorescence scan maps. A following 10min RCA1 cleaning step removed residual organic material and promoted surface hydrophilicity for the subsequent spincoating of ND's (Adámas Nanotechnology) with mean size/number of NV-centers of 40 nm/∼15 suspended in water. Successively, a water suspension of chemically synthesized silver nanocubes (nanoComposix), Fig. 1(b), of mean size 100 nm, encapsulated in a polyvinylpyrrolidone (PVP) layer $\leq$ 5 nm, was spincoated onto the sample. The SE of

Optical Materials EXPRESS

NV-centers in diamond, situated on a low fluorescence fused silica substrate, were excited by a 532 nm linearly polarized pulsed laser (LDH-P-FA-530L - Picoquant) with pulse width/period of ~50 ps/400 ns, Fig. 1(a). A half-wave plate situated in the excitation light path controls the polarization of the pump light, which is focused onto the sample by a ×100 (NA 0.90) objective. The fluorescence, collected by the objective, was filtered by a dichroic mirror (cut-off 550 nm), passed through an analyzer and detected either by a grating spectrometer (SR303i - Andor), equipped with an electron multiplying CCD (IXon Ultra - Andor), or a single photon sensitive photo avalanche diode (APD) (τ-SPAD - Picoquant) connected to a pulse-to-photon arrival timing box (Picoharp 300 - Picoquant). We apply this setup to characterize the spectral and temporal response for various configurations of pump polarization and analyzer. For direct comparison of the spectral power, all measurements were done at an average laser power of 10 μW, using the same acquisition time of 10 min.

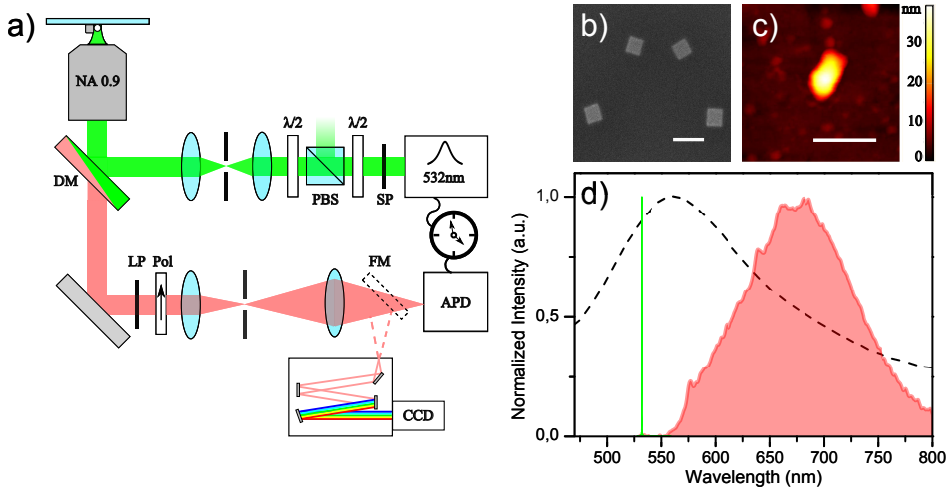

Fig. 1. Schematic of experimental setup for characterization of NV-center SE (a). SP, short pass; LP, long pass filter; PBS, polarizing beam splitter; $\lambda/2$, half-wave plate; DM, dichroic mirror; Pol, analyser; FM, flip mirror. Experimental constituents, scale bar 200 nm, micrograph of silver cubes (b) and AFM scan of ND (c). Spectral properties of individual elements (d) scattering spectra of silver cubes on quartz glass, relative to white paper (dashed), fluorescence spectrum of ND (red) and excitation laser line (green).

The measurements were completed within 72 hours of spincoating the silver cubes, during which time we observed no fluorescence of the cubes, as cubes located with AFM did not show up in our fluorescence scan maps. Scanning the sample with an AFM, we locate a single ND, Fig. 1(c). The diamond emits the characteristic fluorescence spectrum of an NV-center, identified by the zero phonon line peaks for the neutral (575 nm) and negative (637 nm) charge states respectively, Fig. 1(d). Correspondingly, the resonance of the silver nanocube is measured to ~560 nm, based on the scattering spectrum of numerous nanocubes distributed on a glass substrate. Enhancement effects can thus be expected at both the excitation and SE wavelength for the assembled ND-cube system. We place the 30 nm ND, near the center of a cube facet, by only manipulating the 110 nm cube with the AFM, Fig. 2(a). It is worth pointing out that by this approach the ND (and hence NV-center dipole orientation) was unmoved throughout the experiment. For reliable comparison of polarization dependent measurements, cf. the appendix. For reference purposes, we introduce a cartesian coordinate system, with the x-, y-axes parallel with the substrate and the x-axis aligned with the ND-cube axis, normal to the cube facet.

Initially, we do not consider the dependence of SE polarization, by omitting the analyzer in

Optical Materials EXPRESS

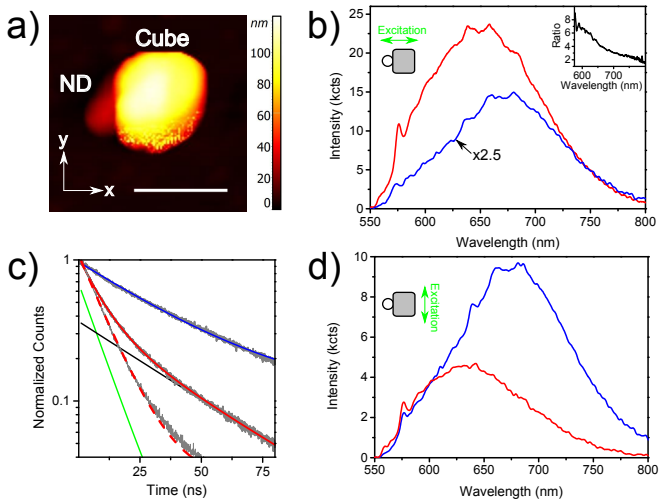

Fig. 2. AFM scan of assembled ND-cube system, scale bar 200 nm (a). The *x*-, *y*-vectors define the reference coordinate axis. Measurements of isolated ND (blue) and ND-cube system (red). Exponential fits of lifetime decay data (c) for x- (solid) and y-polarized pump (dashed). Green and black curve give respectively fast and slow exponential of bi-exponential decay for ND-cube system under x-polarized pump (solid red). Decay curve of isolated ND under y-pump overlays that for x-pump and is omitted for clarity. Corresponding SE spectra for excitation polarized along *x* (b) and *y* (d). Inset give the ND-cube to ND spectral ratio.

the detection light path. For *x*-polarized pump light, Fig. 2(b), the photon rate or fluorescent power (obtained by integration of fluorescence spectrum) of the ND-cube system is enhanced by a factor of 4.1 relative to the isolated ND. The spectral power is increasingly enhanced towards the cube resonance, as NV-centers couple to the LSP-cube mode, effectively increasing decay probability of near-resonance dipole transitions. The excited state lifetime is reduced by a factor of 4.1, evident as the lifetime decay curve goes from single exponential (isolated ND) with a fitted lifetime of 36.1 ns to double exponential (ND-cube) with a fast lifetime component of 8.9 ns, Fig. 2(c). For *y*-polarized pump light, the lifetime reduction is 3.2, Fig. 2(c), while the total fluorescent power is decreased with an enhancement factor of 0.5, Fig. 2(d).

In the following, we consider the polarization dependent properties of NV-center SE. Inserting an analyzer in the detection light path, we measure spectral and temporal SE properties for *x*- and *y*-orientations of analyzer and pump light, Fig. 3. In the case of an *x*-oriented analyzer we recover similar spectrum and decay curves observed for the ND-cube system in the absence of analyzer for x-pump light, Fig. 3(a), with slight differences observed in the spectrum for y-pump light, Fig. 3(c). The similarity is a result of the SE being mainly polarized along the *x*-axis, as respectively 86 % (*x*-pump light) and 93 % (*y*-pump light) of the detected power is *x*-polarized. In contrast, the SE of the isolated ND is preferentially co-polarized with the excitation, as respectively 78 % (*x*-pump light) and 43 % (*y*-pump light) of the emitted photons are *x*-polarized. The polarization of NV-center emission in the presence of the cube, result from excitation of the plasmonic cube mode during NV-center relaxation. The cube mode is a dipole-like mode [34], consisting of charge density oscillations along the ND-cube axis. The energy funnelled from the NV-center into the cube is either ohmically dissipated or scattered to free space in dipolar fashion, polarized along the dipole axis of the cube mode (ND-cube axis). The result is experimentally observed as the apparent polarization of NV-center emission, for NV-centers efficiently coupling to the cube. The efficiency of NV-to-cube energy transfer increases with the NV-center dipole projection on the electric field of the cube mode, oriented perpendicular to the cube surface. For NV-center

Optical Materials EXPRESS

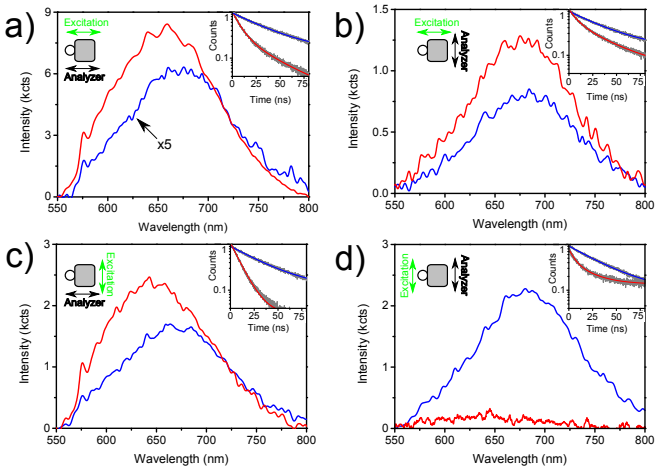

Fig. 3. Polarized SE spectra of isolated ND(blue) and ND-cube system(red). Excitation polarized along x and analyzer orientation, x (a) or y (b). Excitation polarized along y and analyzer orientation x (c) or y (d). Insets give corresponding measurements of lifetime decay curves.

dipoles oriented along this axis, the increased rate at which the NV-center may dissipate energy, given coupling to the cube, is observed as a decrease in lifetime. We note the reduced lifetime and spectral modulations observed for x-oriented analyzer, demonstrate the strongly x-polarized SE result from NV-centers coupling to the LSP mode of the cube. For y-oriented analyzer and x-polarized excitation, Fig. 3(b), the signal can predominately be attributed to NV-centers not coupling to the cube mode, as 78 % of the photons contribute to an exponential decay with a near unchanged lifetime of 35 ns, in agreement with the unmodulated SE spectrum. Finally, for y-polarized pump light, Fig. 3(d), the signal was reduced to an inadequate level for resolving spectral features. The correspondingly weak lifetime decay curve, only slightly above the background of the APD dark count, is included for completeness.

With the purpose of identifying the underlying factors responsible for experimental observations, we numerically model the SE of NV-centers in close proximity to a silver nanocube situated on a glass substrate. As the SE response of an emitter is strongly dependent on dipole orientation, it is initially worth noting the physical dipole configuration of the NV-center. The NV-center consists of a substitutional nitrogen-vacancy pair situated along the $\langle 111 \rangle$ crystal axis in diamond [37]. 4 orientations of the N-V axis are thus possible within the diamond lattice. The excitation and SE of the negatively charged NV-center is facilitated by 2 orthogonal dipole axes, corresponding to the double degenerate excited electronic states, with the dipole axes lying in the plane perpendicular to the N-V axis. At room temperature the population of the excited electronic states completely mix, allowing spontaneous decay by either dipole axes [38]. The modelling of SE from multiple NV-centers, distributed throughout the ND, with different dipole orientation is clearly a complex challenge. In the following we, therefore, limit ourselves to a simplified model by approximating the NV-center as a randomly oriented dipole. Considering the relatively omnidirectional response of the negatively charged NV-center, given the 2-dipole configuration, we consider such an approximation quite reasonable. The most likely response of the ND, is obtained by averaging the modelled dipole response over the ND. Though only qualitative agreement of experiment and model should be expected, the model captures the governing physics of the experiment.

We proceed by a detailed description of the model. The excited NV-center is modelled as an electric dipole, harmonically oscillating at the SE frequency, with the associated point source

Optical Materials EXPRESS

current density $\mathbf{j}_p$, for which unit vector $\hat{\mathbf{n}}_p$ defines the axis of charge oscillation or dipole axis. Assuming unity intrinsic quantum yield, we note the time-averaged power P^{rad} radiated from the volume enclosing the cube and point source is given by the energy dissipation of currents included in the volume [39]. Splitting current terms into the point source driving term and sink terms for the polarization currents induced in the cube, we write:

$$P^{tot} = P^{rad} + P^{nr} \tag{1}$$

where P^{nr} is the power dissipated in the cube by ohmic heating, while the total power dissipated by the point source is given by $P^{tot} = -\frac{1}{2}\mathrm{Re}\{\mathbf{j}_p^* \cdot \mathbf{E}(\mathbf{r}_0)\}$. $\mathbf{E}$ being the electric field, generated by the point source, at the source origin $\mathbf{r_0}$. Assuming the Cartesian dipole components are not coupled, that is, the generated electric field is parallel with the dipole axis at $\mathbf{r}_0$, for an x-,y- or z-oriented dipole, respectively. The power dissipated by the randomly oriented dipole is written as a weighted superposition of contributions from Cartesian dipole components i.e. $P^{tot} = \sum_{x,y,z} g_i P_i^{tot}$. The weighting factors are found to be $g_{\parallel} = 0.6$ for the dipole component parallel with pump polarization and $g_{\perp} = 0.2$ for the orthogonal dipole components, imposed by the photo-selective dipole excitation of the pump light, on the assumption of parallel absorption and emission dipole axis cf. the appendix. In order to model enhancement effects of the fluorescent photon rate, we note the measured lifetime of the isolated ND (36.1 ns) is much longer than the laser pulse duration (~50 ps) and significantly shorter than the pulse period (400 ns). The NV-centers, therefore, decay before the next laser pulse. We thus write the detected photon rate (R), in the non-saturated form, limited by the excitation rate.

$$R = \gamma_{ex}\Phi\eta \tag{2}$$

The excitation rate is given by $\gamma_{ex} \propto |\hat{\mathbf{n}}_p \cdot \mathbf{E}^{ext}(\mathbf{r}_0)|^2$, where $\mathbf{E}^{ext}$ is the electric field generated by an external source (eg. laser) at the excitation frequency. While $\Phi = P^{rad}/P^{tot}$ is the quantum yield and $\eta = P^{obj}/P^{rad}$ the collection efficiency of the objective for the power P^{obj} radiated to the objective. For simplicity, we model the NV-centers distributed within the 30 nm tall ND, by simulating the dipole response for an emission wavelength of 637 nm, over a 30 nm×30 nm area in the xz plane, centred near the facet of a 110 nm cube. Enhancement factors for each point is obtained relative to the response of the dipole above the glass substrate, with reference parameters subscripted by 0. Finally, the enhancement factors most likely to be observed in experiment, are obtained by averaging over the simulated dipole map. The best agreement of experiment and model is found for a 16 nm separation of cube and ND simulation area. Such a separation is quite realistic and the subsequent modelled values are thus simulated under this condition.

Having established the general model, we proceed to identify the parameters responsible for experimental observations by numerical full-wave 3D simulations (using the commercial finite element software Comsol Multiphysics). Material parameters for the 110 nm silver cube with side/corner rounding radius of 7 nm and the fused quartz glass substrate were obtained from tabulated data [40, 41]. Considering the photon rate, Eq. 2, we find virtually unchanged values for the quantum yield and collection efficiency, with average values for the ND-cube system of $\Phi = 0.98, 0.97$ and $\eta = 0.22, 0.20$ for x-, y-polarized pump respectively and $\Phi_0 = 1$, $\eta_0 = 0.17$ for the reference. The enhancement of photon rate, is therefore attributed to an increased excitation rate, resulting from local enhancement of the incident laser field. For x-polarized pump, the field is strongly enhanced at the ND, given the excitation of the LSP mode of the cube (polarized with the pump), well-confined near the substrate, Fig. 4(a). In contrast the excitation field is suppressed under y-polarized illumination, Fig. 4(b), resulting in respectively enhancement and

Optical Materials EXPRESS

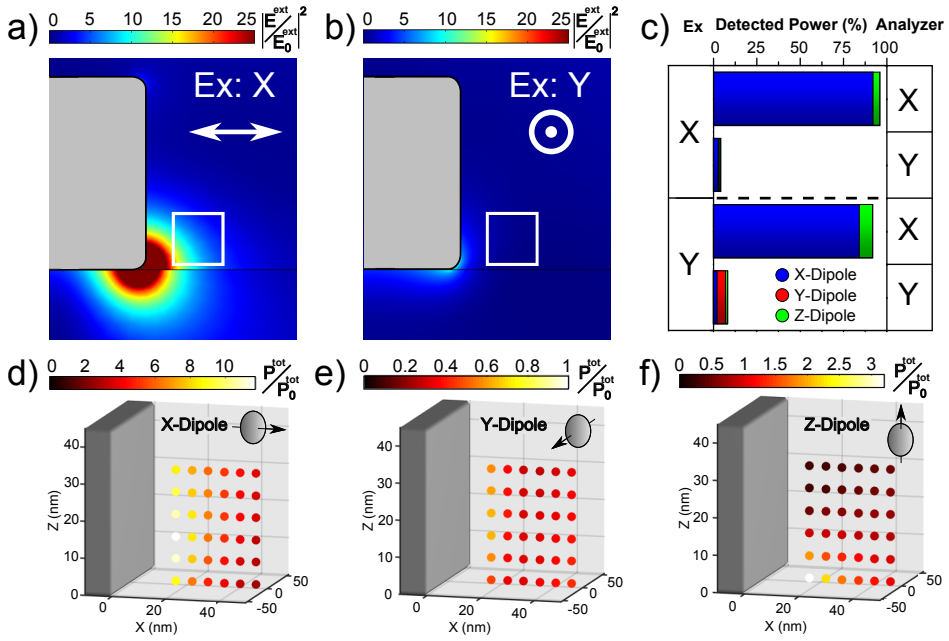

Fig. 4. Simulation of norm squared excitation field generated at by plane wave (wavelength: 532 nm) at normal incidence on silver cube, polarized along x (a) and y (b), relative to field in absence of silver cube. White square indicate the simulated ND area. Contributions of dipole components to average power radiated to objective for randomly oriented dipole (c). Power dissipation of dipole radiating at emission wavelength 637 nm, relative to dipole in absence of cube, for dipole moment orientation x(d), y(e) and z(f), mapped over the ND simulation area.

suppression of the photon rate, in good agreement with experimental observations. Concerning physical effects related to the emission wavelength (eg. radiative decay rate and polarization of fluorescence), we initially consider the power dissipated by x-, y- and z-oriented dipoles in the ND simulation area, Figs. 4(d)-4(f). The power dissipated by an x-oriented dipole is significantly enhanced in close proximity to the cube, as the dipole orientation is well-aligned with the electric field of the LSP mode, while the z-dipole show modest enhancement near the rounded cube corner, the y-dipole is suppressed, presumably due to an anti-phase image dipole induced in the cube facet, limiting dipole radiation by destructive interference [42]. Consequently the reduced lifetime, mainly result from the randomly oriented dipole's projection on the x-axis. The model agrees qualitatively with experiment as a significant decrease in lifetime was observed for x-oriented analyzer, Fig. 3(a) and 3(c), while the lifetime was mainly unchanged for y-aligned analyzer, Fig. 3(b). Finally, we decompose the power radiated into the objective in terms of x- and y-polarization and consider the contributions of the various dipole components to the overall power radiated by the randomized dipole, Fig. 4(c). In order to account for the spatially dependent dipole excitation efficiency, we apply a weighted average for the ND simulation area, using $|E^{ext}|^2$ as weighting function. The power radiated to the objective, is dominated by the efficient power dissipation of the x-dipole component, resulting in strongly x-polarized SE for both x- and y-polarized pump light, in agreement with experimental observations.

We conclude the numeric study by comparing the trend of modelled and experimental enhancement factors, Table 1. Note the modelled value for lifetime reduction, given by (P^{tot}/P_0^{tot}), is obtained by a weighted average over the ND simulation area, using the excitation field as weighting function. Generally the simple model of a randomly orientated dipole emitting at a

Optical Materials EXPRESS

Table 1. Experimental (red) and modelled (blue) values of photon rate enhancement and lifetime reduction.

	Photon rate enhancement			Lifetime reduction
Excitation \ Analyzer	X	Y	÷	÷
X	6.3	1.5	4.1	4.1
	11.6	1.9	8.5	4.2
Y	1.4	0.08	0.5	3.2
	1.8	0.06	0.6	2.0

● Experiment ● Model

single wavelength, follow the trend of experimental values for lifetime reduction and photon rate enhancement, when averaged over the ND. The photon rate enhancement factors observed in experiment, may therefore be interpreted by two polarization dependent factors, enhancement of excitation field and polarized SE resulting from NV-centers coupling to the LSP mode of the cube. For x-oriented analyzer and pump polarization, the excitation field is enhanced at the ND and the analyzer is aligned with the strongly x-polarized SE, resulting in the largest enhancement factor. Rotating either pump or analyzer to y-orientation, either the excitation field is suppressed or the analyzer probe the weak y-polarized SE, resulting in modest enhancement factors for crossed analyzer and pump. In the case of both analyzer and pump parallel with the y-axis, both factors contribute to a strongly suppressed signal. Beyond the simplified model, we qualitatively comment on expected effects not captured by the model. We note the intrinsic quantum efficiency of an NV-center in a ND is in fact not unity [33]. Enhancement of quantum yield by an increase in the radiative decay, in the presence of the cube, may therefore be a contributing factor to the enhancement of photon rate observed experimentally. On the other hand, neglecting the high refractive index of the diamond in the model, is expected to result in an overestimation of the excitation rate and hence photon rate enhancement, as the plasmonic field is typically ”pushed” from the dielectric to the metal side, when increasing the refractive index of the dielectric. Neither effect is however expected to change the polarization dependent tendencies modelled in Table 1.

Lastly, we demonstrate the consistency of our experimental observations by reproducing the ND-cube coupled system for a ND containing few NV-centers. For the few emitter experiment, the setup, Fig. 1(a), was upgraded with a continuous wave 532 nm laser (CL532-100 - Crystal Laser), introduced in the excitation light path by a flip mirror. Excitation and collection was facilitated by a $\times 100$ (NA 1.4) oil immersion objective, while a 50:50 beamsplitter, inserted in the collection light path, passes collected photons to a secondary APD (τ-SPAD - Picoquant), for second order correlation measurements. The second order correlation function ($g^{(2)}(\tau)$) is obtained as an event histogram by accumulating the time delay (τ) for events of a photon arriving on one APD and starting a timer and the arrival of a photon on the other APD stopping the timer. As single quantum emitters may only emit one photon at the time, the zero delay value follow $g^{(2)}(0) = 1 - 1/n$, n being the number of emitters contributing to the signal, assuming no background. The number of NV-centers contained in the 20nm ND, Fig. 5(a), is determined to be 1 or 2, evident as the $g^{(2)}(0)$-value drops to $\sim$0.5, without applying any background correction, Fig. 5(b). The absence of background fluorescence from the silver cube is evident as the $g^{(2)}(0)$-value for the assembled ND-cube system is nearly unchanged from the isolated ND. The lifetime decay curve, Fig. 5(c), is fitted for a bi-exponential decay. We attribute the fast exponential to background, fitted to respectively 4.9ns and 4.1ns for the isolated ND and assembled ND-cube system. The slow exponential, resulting from NV-center emission, drop from 27.9ns for the isolated ND to 11.6ns, after system assembly, giving a lifetime reduction factor of 2.4. The assembly of the ND-cube system, Fig. 5(d), result in the characteristic spectral

Optical Materials EXPRESS

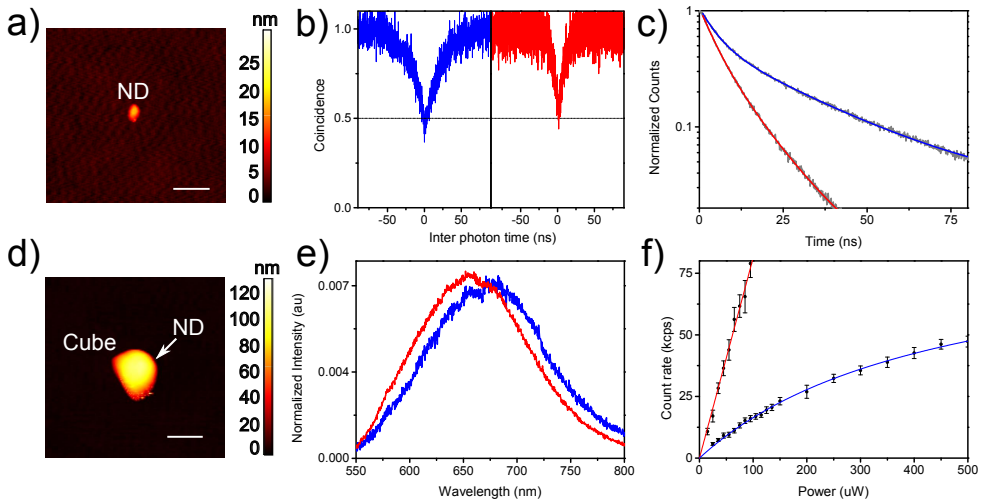

Fig. 5. Few NV-center emission from isolated ND (blue) and assembled ND-cube system (red). AFM scans (a),(d) give the respective configurations, scalebar 200nm. 2. order correlation measurement (b) no background correction applied. Lifetime decay curves fitted to bi-exponentials (c). SE spectra normalized to a spectral area of 1 (e). Saturation model for 2-level system(line) fitted to measured photon count rate (points) as function of laser power (f), errorbar correspond to one standard deviation.

change favouring near cube resonance emission, Fig. 5(e). Measuring the count rate on a single APD as a function of pump power, for pump polarization optimized for maximal count rate, we collect saturation curves for either configuration, Fig. 5(f). The curves are fitted to a saturation model for a 2-level system of the form. $R = R_\infty P/(P + P_s)$, R being the detected count rate, P the laser pump power, P_s the saturation pump power and R_∞ the maximum detectable count rate at infinite pump power. The curves are bounded between a linear non-saturated regime at small laser power, for which the photon rate is limited by the excitation rate of the emitter. In the saturated regime for large laser power, the photon rate is limited by the rate at which the emitter can emit photons into the objective, given the finite lifetime of the excited state. Considering the linear slope for the non-saturated regime, we find the photon rate increases by a factor 4.1 after introducing the cube, in good agreement with the previous experiment. The count rate, for the isolated ND at infinite pump power, is fitted to $R_\infty = 90$ kcps, while the saturation curve for the ND-cube system appear to increase beyond this level. The increase of R_∞ after introducing the cube, suggest the corresponding reduction of lifetime result from an increase in radiative decay rate, given coupling to the cube, rather then quenching.

3. Conclusion

In summary, we have studied the SE properties of NV-centers in close proximity to a silver nanocube relative to a homogeneous environment, by deterministic assembly of a single ND-cube system using an AFM. The SE from the assembled system is strongly polarized along the x-axis, intersecting the ND and cube, while the rate of emitted photons strongly depend on the polarization of the pump laser. For optimal pump, the photon rate is enhanced by a factor of 4.1, while the excited state lifetime is reduced by a factor of 4.1. Separating fluorescence spectrum and lifetime decay curves into x- and y-polarization; the strongly x-polarized SE is attributed to NV-centers coupling to the LSP mode of the cube, while a weak y-polarized signal is attributed to uncoupled NV-centers. The physics observed in experiment is qualitatively reproduced by modelling, the ND averaged, response of a randomly oriented electric dipole. Based on the model,

Optical Materials EXPRESS

we identify the total photon rate enhancement to result from local field enhancement of the pump laser and potentially increased quantum yield, while the reduction in lifetime is a consequence of NV-centers coupling to the LSP mode of the cube. The consistency of experimental results was further demonstrated by the coupling of a ND containing few NV-centers to a silver nanocube. The results provide a foundation for incorporating NV-centers into more complex cube-based photon sources.

Optical Materials EXPRESS

Appendix

Nanodiamond orientation

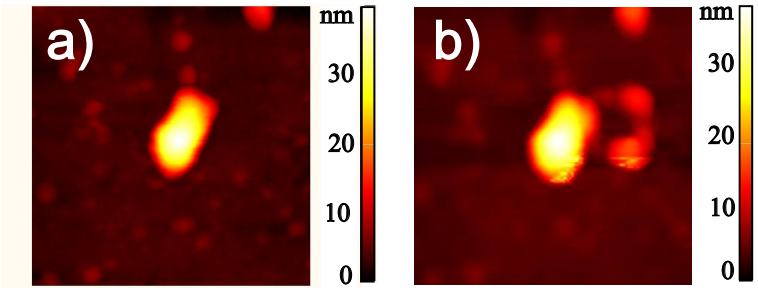

Fig. 6. AFM scan of ND as initially characterized, before moving silver cube (a) and complementary scan after, moving silver nanocube to ND, characterization and finally cube pickup with AFM (b). The ND orientation appear unchanged throughout the experiment.

Power dissipation by randomly oriented dipole

In the following we calculate the average dipole components of an excited dipole for a random absorption dipole orientation. The power dissipated by the dipole at the emission wavelength is expressed as a superposition the power dissipated by respective an x, y or z oriented dipole moment, weighted by the average dipole components of the excited dipole.

We specify the vector for the absorption dipole moment in spherical coordinates with azimuthal angle φ and inclination angle θ. The probability of finding the absorption dipole in the interval $[\theta, \theta + d\theta; \varphi, \varphi + d\varphi]$, is given by the differential surface area of a sphere, relative to the total area.

$$f(\theta)d\theta d\varphi = \frac{\sin(\theta)d\theta d\varphi}{4\pi} \tag{3}$$

We consider the electric excitation field oriented along the cartesian z-axis, and note the probability, the excitation field will excite the dipole, is proportional to the squared norm of the absorption dipole projection on the excitation field. The probability of finding the excited dipole in the interval $[\theta, \theta + d\theta; \varphi, \varphi + d\varphi]$ is thus given by:

$$f_{ex}(\theta)d\theta d\varphi = C\frac{\sin(\theta)\cos^2(\theta)d\theta d\varphi}{4\pi} \tag{4}$$

C being the normalization factor, such that $1 = \int_0^{2\pi}\int_0^{\pi} f_{ex}d\theta d\varphi$. Expressing the excited dipole moment in cartesian components.

$$\mathbf{p} = |p|(\hat{\mathbf{n}}_x \cos(\varphi)sin(\theta) + \hat{\mathbf{n}}_y \sin(\varphi)sin(\theta) + \hat{\mathbf{n}}_z \cos(\theta)) \tag{5}$$

We calculate the average norm squared components of the excited dipole.

Optical Materials EXPRESS

$$\left\langle |p_x|^2 \right\rangle = \int_0^{2\pi} \int_0^{\pi} |p_x(\theta,\varphi)|^2 f_{ex}(\theta) d\theta d\varphi = g_x |p|^2 \tag{6}$$

$$\left\langle |p_y|^2 \right\rangle = \int_0^{2\pi} \int_0^{\pi} |p_y(\theta,\varphi)|^2 f_{ex}(\theta) d\theta d\varphi = g_y |p|^2 \tag{7}$$

$$\left\langle |p_z|^2 \right\rangle = \int_0^{2\pi} \int_0^{\pi} |p_z(\theta)|^2 f_{ex}(\theta) d\theta d\varphi = g_z |p|^2 \tag{8}$$

Weighting factors being respectively, g_z=0.6 for dipole component parallel with excitation field and g_x=g_y=0.2 for dipole components orthogonal to excitation. Assuming the absorption dipole axis (ie. dipole axis at the excitation wavelength) is parallel with the emission dipole axis (ie. dipole axis at the emission wavelength), we express the emission dipole unit vector ($\hat{\mathbf{n}}_p$), interims of the average excited dipole orientation.

$$\hat{\mathbf{n}}_p = (\hat{\mathbf{n}}_x \sqrt{g_x} + \hat{\mathbf{n}}_y \sqrt{g_y} + \hat{\mathbf{n}}_z \sqrt{g_z}) \tag{9}$$

The power dissipated by the radiating dipole oscillating at the emission frequency, is given by the classical expression [39].

$$P^{tot} = \frac{\omega^2 |p|^2}{2c^2 \varepsilon_0 \varepsilon} \left(\hat{\mathbf{n}}_p \cdot Im\{\overleftrightarrow{\mathbf{G}}(\mathbf{r}_0, \mathbf{r}_0, \omega)\} \cdot \hat{\mathbf{n}}_p \right) \tag{10}$$

ω being the emission frequency, c the vacuum speed of light, ε_0 the vacuum permittivity, ε the permittivity of the medium and $\overleftrightarrow{\mathbf{G}}$ Green's dyadic evaluated at the dipole location $\mathbf{r}_0$. Assuming no coupling of the cartesian dipole components, that is the Green dyadic only contain diagonal elements, as the electric field (evaluated at $\mathbf{r}_0$) generated by an x-,y or z-oriented dipole, is parallel with the respective dipole axis. We express the total power dissipated by the dipole, as a superposition of the power dissipation for a x,y and z oriented dipole, weighted by the corresponding weighting factor.

$$P^{tot} = \frac{\omega^2 |p|^2}{2c^2 \varepsilon_0 \varepsilon} \left(\sum_{i=x,y,z} g_i \hat{\mathbf{n}}_i \cdot Im\{\overleftrightarrow{\mathbf{G}}(\mathbf{r}_0, \mathbf{r}_0, \omega)\} \cdot \hat{\mathbf{n}}_i \right) \tag{11}$$

Funding

European Research Council (Grant 341054 (PLAQNAP)).